Acta Geotechnica Slovenica

LOADING-MODE INTEGRITY AND CONSERVATIVE AFFINE REDUCTION OF WETTING-SENSITIVE IMPROVED FILL

Aditya Pratama[1], Dewi Anggraini[1], Rizky Saputra[1] and Nadia Putri[2,*]

[1] Geotechnical Engineering Research Group, Faculty of Civil and Environmental Engineering, Institut Teknologi Bandung, Bandung, Indonesia

[2] Department of Civil and Environmental Engineering, Faculty of Engineering, Universitas Indonesia, Depok, Indonesia

Received: 12/6/2026 Revised: 05/10/2026 Accepted: 25/10/2026 Published: 5/11/2026

***Correspondence:** nadiaputri@ui.ac.id

DOI: 10.68304/gsej2026.a107

ABSTRACT

Representing improved fill with a single Mohr–Coulomb parameter set can combine different loading modes or overlook a change in which mode provides the lower resistance as confinement increases. This study examines whether a conservative tuple can be defined over a specified confinement interval while retaining the reported origin of each parameter pair. A 2025 experimental programme on ash-bound colliery spoil provides eight documented series-level tuples, two alternative dry-state reports and four numerical-model inputs. Common-strain work, incomplete-curve bounds, constrained integration and shared calibration form a separate measurement-level layer. The parameter-level comparison combines a reporting-location audit, exact loading-mode crossover analysis, demand-disagreement sets, bounded parameter propagation and optimal conservative affine reduction. Wet-mode crossovers occur at 482.08 kPa under total-stress parameterization and 222.26 kPa under the interpreted effective-stress parameterization. Over the analytical interval of 0–500 kPa, one documented total-stress model input understates the lower mode prediction by up to 28.09%. The selected effective-stress input exceeds its corresponding lower mode prediction by 13.85% at the upper endpoint. Optimal affine reductions give $(c, \phi) = (40.158\ \text{kPa}, 34.815°)$ and $(138.710\ \text{kPa}, 31.900°)$, with mean deviator-resistance deficits of 6.982 and 49.885 kPa, respectively. These results quantify the cost of conservative reduction over a declared domain while retaining unresolved differences among reports.

Keywords: improved fill; loading control; parameter parameter origin; wetting sensitivity; conservative model reduction; confinement dependence

© 2026 The Author(s). Published under the CC BY 4.0 license.

1. INTRODUCTION

Ground improvement is increasingly assessed through evidence assembled across material preparation, laboratory testing and numerical modelling rather than through a single directly observed performance measure. This is especially important when industrial by-products are used as fill or as reactive binders. Their reuse can reduce demand for natural aggregates, but geotechnical suitability still depends on the treated material's response to loading, moisture and time. The literature on anthropogenic soils demonstrates that engineering classification must reflect their measured properties rather than their origin alone [1]. Investigations of colliery spoil as road subbase likewise connect reuse opportunities with material characterization and application-specific requirements [2]. An acceptable route to reuse therefore needs both a defensible material description and a transparent account of how that description becomes an input to analysis.

Ash-bearing materials illustrate why this translation is consequential. A review of fly-ash and colliery-spoil blends identifies compaction, strength and stability as connected aspects of their geotechnical assessment [3]. However, ash from fluidized bed combustion should not automatically be equated with conventional pulverized-coal fly ash. Its composition and utilization characteristics can differ substantially, with implications for the reactions that develop after mixing [4]. The present study concerns one specific ash-bound spoil mixture rather than a universal class of coal-derived materials. This distinction prevents a broad environmental argument for reuse from becoming an unsupported claim that all waste-derived fills share the same mechanical behaviour or durability.

The contribution of a reactive binder also depends on the conditions under which its effects develop. Chemical stabilization research identifies additive chemistry, soil mineralogy, water content, curing and deleterious constituents as relevant influences on performance [5]. A broader review of stabilization methods similarly places durability alongside initial improvement rather than treating early strength as a sufficient endpoint [6]. In spoil–bottom-ash mixtures, swelling and confinement-dependent behaviour provide additional reasons to distinguish material formation from subsequent service conditions [7]. These observations motivate careful interpretation of a tabulated strength pair: the pair represents a particular material state and test procedure, not an intrinsic description independent of preparation or exposure.

Water exposure is particularly difficult to compress into one reduction factor. In cement-treated sand, the mechanical consequences of wetting and drying depend on the imposed cycling protocol and binder dosage [8]. Studies of successive hydric cycles also examine strength together with hydraulic conductivity, demonstrating the value of evaluating more than one aspect of treated-soil performance [9]. Freeze–thaw and wetting–drying investigations extend this concern to volumetric and hydromechanical changes [10]. These findings do not supply correction factors for the material analysed here. They establish why an observation made after one inundation event should not be extrapolated automatically to repeated weathering, another binder or an unrestricted field exposure history.

Laboratory strength is also conditioned by the loading process. Unsaturated silty-clay tests

explicitly investigate strain-rate dependence across different confinement levels [11]. Rate-controlled triaxial investigations of reconstituted unsaturated soil connect measured response with both suction and the chosen deformation rate [12]. More recent drained-vented testing addresses the interaction of initial saturation, shearing rate and pore-pressure dissipation [13]. Consequently, differing stress-rate and strain-rate series cannot simply be regarded as exchangeable replicates. A comparison must retain the mode label and acknowledge that a constant shortening rate and a constant stress rate do not impose identical trajectories through a nonlinear or brittle response.

A related distinction separates a material law from its numerical reduction. Constitutive models for cemented sand can represent stiffness enhancement, dilatancy and progressive bond degradation within one evolving formulation [14]. Research on the stress-path dependence of weakly cemented sand and on stress–dilatancy descriptions of bonded soils likewise addresses information beyond a peak-strength envelope [15, 16]. By contrast, many practical calculations retain a small number of Mohr–Coulomb parameters. Such a reduction can be useful, but its limited purpose should remain explicit. It does not recover strain softening, hydraulic response, rate dependence or work absorption merely because it matches selected strength observations.

Equivalent linear parameters are already used over specified stress ranges in engineering software [17]. The choice of range matters because the fitted line is an approximation to behaviour over that range rather than a universal material constant. The question pursued here differs from ordinary best fitting. Instead of minimizing an average residual around a nonlinear envelope, the proposed reduction must remain below every admissible loading-mode prediction throughout a declared interval. Its objective is then to preserve as much interval-average predicted resistance as possible. This creates a precise comparison between convenience, conservativeness and the resistance sacrificed by using one affine representation.

Uncertainty complicates the selection further. A linear regression used to estimate cohesion and friction introduces dependence between fitted quantities and does not make their confidence limits interchangeable with physical strength limits [18]. Investigations of dependence structures in sandy-clay parameters show why independently selecting coordinate extremes can fail to preserve the original statistical relationship [19]. Geotechnical uncertainty also includes model inadequacy, interpretation and incomplete characterization, not only spatial material variation [20]. These categories should not be merged into one unsupported error bar. In particular, contradictory values at two locations in a publication are reporting alternatives until resolved, rather than a random sample from an estimated measurement-error distribution.

The present study preserves the distinction between observation-level and parameter-level information. Nominal axial stress integrated against engineering strain supplies an external-work quantity when specimen geometry, displacement and calibration are known. Work comparisons require a common strain window and an explicit treatment of incomplete records. A cohesion–friction tuple supplies a different object: the predicted failure resistance of its stated relation. It cannot reconstruct the curve from which it was inferred. Both information levels are considered here, but calculations are performed only where the available strength values supports them. This prevents a numerical model of peak resistance from being presented as measured deformation energy or as an independently observed treatment effect.

The central research question is whether one Mohr–Coulomb tuple can remain conservative relative to all admissible loading-mode predictions over a stated confinement domain without disguising the parameter origin of the input pairs. A connected question concerns the cost of that simplification: how much predicted resistance is lost, and where within the domain does that loss occur? The analytical answer is developed alongside a reporting-location audit of one triaxial programme. The analysis treats complete tuples as admissible alternatives, derives their exact mode-switch coordinates, locates disagreement between a selected input and the lower mode prediction, and solves a constrained affine-reduction problem.

It supplies a calculation procedure from an available parameter record to domain-specific comparison and reduction, while retaining measurement-level work methods for future curve-based validation. Triaxial strength parameters, stipulated sensitivity allowances and mathematical verification cases remain distinct throughout. The resulting calculations can reveal when one tested loading mode ceases to provide the lower prediction, when a componentwise minimum is unnecessarily restrictive under a declared objective, and when an apparently convenient input is not conservative relative to the admissible set.

2. MATERIAL AND TRIAXIAL TEST CONDITIONS

2.1 MIXTURE PREPARATION AND SPECIMEN COUNTS

Triaxial testing of compacted colliery spoil–bottom-ash fill examined the effects of inundation under stress-controlled and strain-controlled loading, with strength interpreted in total and effective stresses [21, 22]. The calculations below use the cohesion–friction pairs from that investigation. Individual stress–strain histories have not been independently checked; consequently, the strength comparisons do not establish deformation energy or specimen-level variability.

The compacted spoil–bottom-ash mixture was cured for 60 days and tested before or after 36 h inundation. Measured water content is approximately 14.6% before inundation and 20–25% afterwards. Loading uses a stress rate of 60 kPa/min or shortening rate of 0.2 mm/min, with total confinement spanning 0–500 kPa. The analysed variables are cohesion c in kPa, friction angle ϕ in degrees, state, mode, interpretation and reporting location.

The programme comprises 21 physical specimens, 18 appearing in the triaxial schedule. Repeated dry/wet schedule entries are not additional independent specimens. The eight interpreted series tuples are not independent treatment replicates. The available record supports deterministic consistency calculations, but not a population wetting-effect variance or confidence interval. Preparation-batch differences likewise prevent treating it as a balanced randomised experiment.

2.2 REPORTING ALTERNATIVES AND COORDINATE INTERPRETATION

Table 1 gives the input. Narrative dry TSA cohesions are 50 kPa above the summary-table values. Both versions remain alternatives; neither is declared correct. The TSA wet model input combines

the smaller cohesion and friction angle from different loading modes. This can be a deliberate conservative selection, but it is not a complete wet-series tuple. The ESA wet model input retains the strain-rate tuple. S and E denote stress-rate and strain-rate control. Entries are $(c\,[\mathrm{kPa}], \phi\,[^\circ])$.

TSA and ESA denote the source's total- and effective-stress interpretations. Its effective correction is indicative because suction and saturation during shearing were not fully established. Here x is a screening coordinate: total minor principal stress under TSA and the interpreted effective minor-stress coordinate under ESA. Equal numerical coordinates do not imply equal physical states. The ESA interval 0–500 kPa is declared for analytical comparison, not verified as measured effective-confinement coverage.

TABLE 1. AVAILABLE PARAMETER RECORD.

Location	Interpretation	State	S	E
Summary	TSA	Dry	(330, 35)	(360, 35)
Summary	TSA	Wet	(160, 29)	(40, 35)
Summary	ESA	Dry	(260, 35)	(290, 35)
Summary	ESA	Wet	(200, 29)	(130, 35)
Narrative	TSA	Dry	(380, 35)	(410, 35)
Model input	TSA	Dry	(380, 35)	
Model input	TSA	Wet	(40, 29)	
Model input	ESA	Dry	(290, 35)	
Model input	ESA	Wet	(130, 35)	

3. AXIAL WORK AND INTEGRATION BOUNDS

3.1 COMMON-STRAIN WORK AND INTEGRATION UNCERTAINTY

For axial force F, initial area A_0, height L_0 and specimen shortening u, nominal stress $s = F/A_0$ and engineering strain $e = u/L_0$ give

$$W_i(t) = \frac{1}{A_0 L_0} \int_0^{u(t)} F \,\mathrm{d}u = \int_0^t s_i(e) \,\mathrm{d}e. \tag{1}$$

The endpoint t is common to compared curves. Percentage strain is divided by 100; kPa integrated against dimensionless strain gives $\mathrm{kJ/m^3}$. Seating, compliance and area corrections require documentation. External work is not automatically dissipation or fracture energy; a peak-strength tuple cannot supply it.

For ordered nodes on one loading branch, the linear interpolant gives

$$\widehat{W}_i(t) = \sum_{k=0}^{m-1} \frac{y_{ik} + y_{i,k+1}}{2} (e_{k+1} - e_k) = \boldsymbol{w}^T \boldsymbol{y}_i, \qquad \sum_k w_k = t. \tag{2}$$

Endpoint insertion is confined to measured support. Duplicate records require verification; different loading branches are not averaged. With uniform stress-error bound δ_i and between-node integral

allowance E_i,

$$W_i(c_i) \in [\widehat{W}_i(c_i) - \delta_i c_i - E_i,\ \widehat{W}_i(c_i) + \delta_i c_i + E_i]. \tag{3}$$

This follows by integrating the absolute stress-error bound. Under justified curvature bounds $|s_i''| \le M_k$ on intervals of width h_k, the trapezoidal allowance is at most $\sum_k M_k h_k^3/12$. Otherwise the computed value is exact only for its interpolant. Uncertain strain coordinates require optimisation over their admissible ordered set; stress-only error does not cover them.

3.2 TRUNCATION, CONSTRAINED INTEGRATION AND ORDERING

For a record ending at $c_i < t$, assume nonnegative stress and an independently justified tail envelope U_i. Then

$$L_i = \max(0, \widehat{W}_i(c_i) - \delta_i c_i - E_i), \tag{4}$$

$$H_i = \widehat{W}_i(c_i) + \delta_i c_i + E_i + \int_{c_i}^{t} U_i(e)\,\mathrm{d}e. \tag{5}$$

A nonincreasing continuation permits a terminal stress upper bound as constant U_i only when that assumption is supported. A measured peak does not bound every unseen hardening branch.

For a nonempty compact polytope of admissible nodal stresses $\mathcal{P}_i$, exact bounds within the declared piecewise-linear class are

$$L_i^{\mathrm{PL}} = \min_{\boldsymbol{z}\in\mathcal{P}_i} \boldsymbol{w}^T\boldsymbol{z}, \qquad H_i^{\mathrm{PL}} = \max_{\boldsymbol{z}\in\mathcal{P}_i} \boldsymbol{w}^T\boldsymbol{z}. \tag{6}$$

Continuity gives attained extrema; convexity makes intermediate values attainable. Additional physical variation between nodes requires further constraints or an allowance. Empty feasible sets are tabulated rather than silently repaired.

For two specimens, $W_B - W_A \in [L_B - H_A, H_B - L_A]$. Thus $L_B - H_A > m$ suffices for advantage $m \ge 0$. Necessity additionally requires sharp, jointly admissible extremes. Overlap means unresolved ordering, not equivalence.

3.3 CALIBRATION DEPENDENCE, ENDPOINT CHECKS AND SAMPLE MEANS

For $y_i = (1+g)s_i + b + r_i$, with common bias b, $|g| \le \gamma < 1$ and $|r_i| \le \rho_i$, equal windows give

$$W_B - W_A = \frac{Y_B - Y_A - (R_B - R_A)}{1+g}, \quad Y_i = \int_0^t y_i\,\mathrm{d}e,\ R_i = \int_0^t r_i\,\mathrm{d}e, \quad |R_B - R_A| \le (\rho_A + \rho_B)t. \tag{7}$$

The additive term cancels only for matched windows and the stated commonality. Bounds follow from numerator endpoints and $1 \pm \gamma$. Such dependence requires calibration evidence. Metrological uncertainty differs from sampling variability and disagreement among reporting locations [23].

For a cumulative nominal difference $D(t)$, extrema occur at knots, boundaries and interior roots of $y_B - y_A = 0$. For the lower envelope $G(t) = D(t) - r(t)$, the condition instead becomes

$y_B - y_A - r'(t) = 0$, including boundaries and nondifferentiable points. A finite treatment mean has bounds $[n^{-1}\sum_i L_i, n^{-1}\sum_i H_i]$ without an independence requirement; these are not population confidence intervals.

These measurement-level methods are specified analytically. Their empirical use requires verified specimen curves, which the present parameter input does not supply. No work is imputed to the fill. A mathematical verification function checks the integration implementation separately.

4. STRENGTH ENVELOPES AND AFFINE REDUCTION

4.1 COMPLETE TUPLES AND TRIAXIAL RESISTANCE

Represent each report by $(c, \phi, \text{state}, \text{mode}, \text{interpretation}, \text{location})$. Retained reports form a set of complete tuples rather than the Cartesian product of coordinate values. Deliberate model hybrids remain analysable but are labelled separately from observed series.

The conventional axisymmetric Mohr–Coulomb relation implies

$$q_f(x) = a + bx, \quad a = \frac{2c\cos\phi}{1-\sin\phi}, \quad b = \frac{2\sin\phi}{1-\sin\phi}. \tag{8}$$

Starting from $(\sigma_1 - \sigma_3) = (\sigma_1 + \sigma_3)\sin\phi + 2c\cos\phi$ and substituting $\sigma_1 = q_f + x$, $\sigma_3 = x$, gives Eq. (8). It predicts a tabulated relation, not individual failure observations. TSA and ESA are transformed separately.

A useful consequence of the tuple representation is that parameter origin becomes part of the admissible set rather than a note appended after calculation. If two parameters were estimated together from one series, their pairing remains intact in the primary comparison. A separate reporting alternative may enlarge the set, but it does not increase the number of independently prepared specimens. This differs from a statistical population model, in which a joint distribution and sampling design would be required. The distinction is consistent with work on parameter identification from field measurements, where transformation uncertainty and spatial description are separate from the measured signal itself [24].

Similarly, a better regression procedure does not by itself resolve a reporting-location conflict. Generalized least squares can address particular residual covariance assumptions when the underlying observations and model are available [25]. In their absence, selecting a favoured parameter value because it improves a subsequent prediction would entangle data reconstruction with the desired conclusion. The primary calculation therefore preserves both dry-state reports and reports their consequences separately. This rule is an evidence-handling decision, not an assertion that the alternatives are equally likely or that the true value lies uniformly between them.

The pressure domain is an explicit input to the reduction problem. It should ideally be selected from the application and supported by the tests before the preferred tuple is calculated. A broader interval may include a change of controlling mode that a narrow interval excludes. Conversely,

extrapolating the fitted laws merely to obtain a more convenient equivalent tuple would reverse the appropriate reasoning. The numerical domain in this study is an analytical screening choice, and the separate qualification of the effective-stress coordinate remains essential. Its endpoints are not characteristic stresses for a real embankment, nor is the uniform weighting in the objective an observed distribution of stress occurrence.

4.2 MODE SWITCHES AND DEMAND DISAGREEMENT

For stress-rate and strain-rate lines $q_S = a_S + b_S x$, $q_E = a_E + b_E x$, define

$$L(x) = \min\{q_S(x), q_E(x)\}, \qquad x_\times = \frac{a_S - a_E}{b_E - b_S} \quad (b_E \neq b_S). \tag{9}$$

Only a crossover inside the selected domain changes the active lower mode. Equal slopes give a fixed mode or coincident lines. Conservatism refers to the admissible predictions, not future specimens or unknown states.

For a selected model input q_M, its signed relative difference is

$$d_M(x) = 100[q_M(x)/L(x) - 1], \qquad L(x) > 0. \tag{10}$$

On an active affine segment, the derivative of this ratio has constant numerator. Its extrema occur at boundaries or mode switches, so maximum discrepancies can be evaluated exactly. For an illustrative deviator demand q_d, disagreement occupies

$$\mathcal{D} = \{(x, q_d) : L(x) < q_d \leq q_M(x)\}. \tag{11}$$

This diagnoses parameter selection; it is not a safety criterion without a real demand field, model validation and justified resistance factors.

4.3 OPTIMAL CONSERVATIVE AFFINE REDUCTION

Software may require one tuple instead of a piecewise envelope. Among affine predictions $\ell(x) = A + Bx$ with $A, B \geq 0$, consider

$$\max\left(A + \frac{BH}{2}\right) \quad \text{subject to } A + Bx \leq q_m(x) \quad \forall m,\ x \in [0, H]. \tag{12}$$

The objective is interval-average predicted q, in kPa. An integral over confinement is not mechanical work and must not be confused with Eq. (1).

Proposition 4.1 (Optimal endpoint chord)**.** *For nonnegative nondecreasing affine mode predictions and $H > 0$, the unique solution is*

$$A^* = L(0), \qquad B^* = [L(H) - L(0)]/H. \tag{13}$$

Proof. The minimum of affine functions is concave, so its endpoint chord lies below it and is

feasible. Every feasible affine function has endpoint values bounded by $L(0)$ and $L(H)$. Its interval mean is half the sum of those endpoints. The chord attains both limits, maximising the mean. Equality requires both endpoints to attain the limits, uniquely determining the line. □

Each difference $q_m - \ell$ is affine; checking nonnegativity at both endpoints is therefore sufficient over the whole interval. Eq. (12) reduces to a two-variable linear programme, providing an independent verification of the closed form.

The affine coefficients correspond to

$$\phi^* = \arcsin \frac{B^*}{B^* + 2}, \qquad c^* = \frac{A^*(1 - \sin \phi^*)}{2 \cos \phi^*}. \tag{14}$$

The tuple is derived, not observed, and optimal only under the declared objective and constraints. For two lines crossing once in $(0, H)$, the nonnegative sacrifice $g = L - \ell^*$ is triangular:

$$g_{\max} = |b_E - b_S| \frac{x_\times (H - x_\times)}{H}, \qquad \overline{g} = H^{-1} \int_0^H g(x)\, \mathrm{d}x = g_{\max}/2. \tag{15}$$

These expressions follow from the linear difference on either side of the crossover. Without an active interior switch, the lower prediction is already affine and the deficit is zero. Multiple modes require every active switch and exact piecewise integration.

4.4 INPUT BOUNDS AND ALTERNATIVE-REPORT RETENTION

For stipulated rectangles $c \in [c_m^-, c_m^+]$, $\phi \in [\phi_m^-, \phi_m^+]$, with $c, x \geq 0$ and $0 \leq \phi < 90°$, Eq. (8) increases with both parameters. A lower mode line therefore uses (c_m^-, ϕ_m^-). Reduce their lower envelope using the same theorem. Rectangles relax within-mode dependence and carry no probability; known dependence should instead be preserved in the admissible set.

The demonstration uses $\Delta c = 5$ kPa and $\Delta\phi = 0.5°$, not measured precision inferred from printed digits. Location disagreement is treated as discrete alternatives. Within-mode wet/dry retention is

$$R_m(x) = \frac{a_{m,w} + b_{m,w} x}{a_{m,d} + b_{m,d} x}. \tag{16}$$

Its derivative likewise has constant sign on a domain with positive denominator, so endpoint evaluation suffices. No causal decomposition of degradation follows from this ratio.

5. RESULTS AND DISCUSSION

5.1 CONFINEMENT-DEPENDENT LOADING-MODE CONTROL

TSA wet lines have $(a_S, b_S) = (543.252198, 1.882060067)$ and $(a_E, b_E) = (153.678570, 2.690172332)$, with intercepts in kPa and dimensionless slopes. Thus

$$x_{\times,\mathrm{TSA}} = \frac{543.252198 - 153.678570}{2.690172332 - 1.882060067} = 482.078598 \text{ kPa}. \tag{17}$$

ESA intercepts are 679.065248 and 499.455353 kPa with the same respective slopes, giving $x_{\times,\mathrm{ESA}} = 222.258593$ kPa. The strain-rate report is lower below each crossover and the stress-rate report above it. This is a property of tabulated lines, not a measured transition of failure mechanism.

The crossover demonstrates why ordering by a single coordinate of the parameter tuple is incomplete. The strain-rate series has the smaller cohesion in both interpretations, yet its larger friction angle gives a steeper confinement dependence after transformation. Close to zero confinement, the intercept controls the difference. As confinement increases, the slope contribution accumulates until the stress-rate series becomes the lower prediction. Neither series is therefore uniformly identified as the more conservative one merely by inspecting cohesion. The conclusion concerns the tabulated relations and does not imply that the laboratory loading mechanism physically changes at the calculated intersection.

This result should also be distinguished from fitted-parameter uncertainty. Correlation between regression coefficients can affect the uncertainty of a predicted strength even when the individual parameter estimates appear well constrained [18]. Dependence models address a different question from selecting the minimum of two tabulated mode predictions [19]. Here the mode label describes a distinct testing condition admissible in the admissible set. Treating the two lines as a random parameter sample, or assigning them equal probabilities without evidence, would add assumptions that the source does not establish. The deterministic envelope avoids that addition while making its own limited guarantee explicit.

The difference between the two crossover coordinates is not a direct estimate of suction influence. Total and interpreted effective coordinates differ in their interpretation, and the source correction does not establish an identical physical path for both. Contemporary unsaturated-soil testing and rate-dependent constitutive work indicate that water pressure, hydraulic equilibration and deformation rate can interact [13, 26]. The present transformation preserves the source labels instead of converting that literature into a numerical correction. A physical explanation of the coordinate difference would require the original stress paths, pore-pressure records and a supported unsaturated effective-stress formulation.

5.2 SELECTED-INPUT CONSEQUENCES

Table 2 compares complete mode predictions with the numerical-model inputs. The TSA hybrid $(40, 29)$ lies below both modes. Its largest relative deficit is 28.0885%, at the crossover. This is conservatism against the admissible set, not proof that the selected input was mistaken or that a field response has that error.

TABLE 2. DERIVED LOWER-MODE PREDICTION L AND SELECTED MODEL-INPUT PREDICTION q_M, IN KPA.

x	TSA L	TSA q_M	ESA L	ESA q_M
0	153.679	135.813	499.455	499.455
50	288.187	229.916	633.964	633.964
200	691.713	512.225	1037.490	1037.490
350	1095.239	794.534	1337.786	1441.016
500	1484.282	1076.843	1620.095	1844.542

The ESA selected tuple $(130, 35)$ is the lower prediction up to 222.2586 kPa. Above that coordinate it exceeds the stress-rate prediction, reaching

$$1844.541519 - 1620.095281 = 224.446238 \text{ kPa}, \qquad 100\frac{224.446238}{1620.095281} = 13.8539\% \tag{18}$$

at 500 kPa. Figure 1 shows the demand-disagreement region. At $x = 350$ kPa, an illustrative demand of 1400 kPa is below the selected prediction, 1441.016 kPa, but above the lower mode prediction, 1337.786 kPa. This distinction does not classify an actual embankment as safe or unsafe. ESA demand coordinates where the selected input and lower mode prediction give different inequality outcomes.

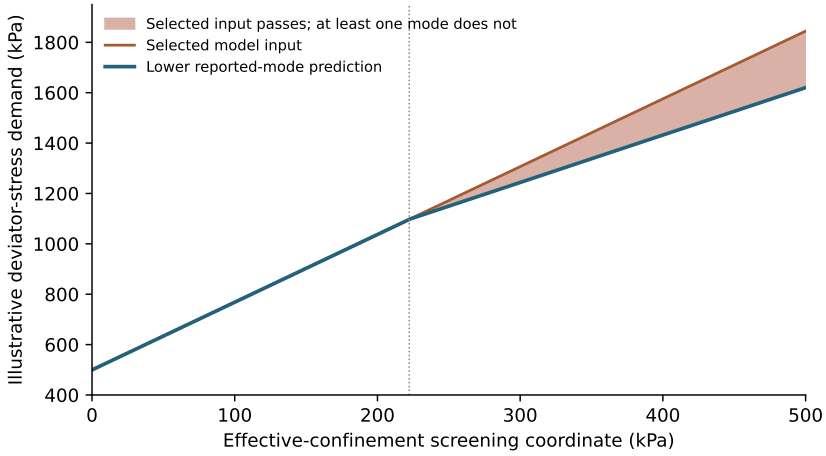


FIGURE 1. ESA DEMAND COORDINATES WITH DIFFERING INEQUALITY OUTCOMES.

The TSA comparison is informative because the hybrid input is not simply the less favourable of two measured tuples. It combines the smaller cohesion from one wet series with the smaller angle from the other. Since predicted resistance increases with both parameters in the stated compression domain, that hybrid lies below both complete predictions. Such a choice can be defensible as a

deliberate conservative simplification. The numerical deficit quantifies the consequence of that choice, rather than identifying it as a transcription error. A report should describe the selection rule so that a reader can distinguish intentional conservativeness from an apparent measured material state.

The opposite issue arises for the selected ESA tuple. It is an actual tabulated mode pair, but that parameter origin alone does not make it the lower prediction everywhere. Beyond the crossover, its steeper slope gives larger resistance than the stress-rate pair. Figure 1 therefore separates two requirements that are sometimes conflated: using an observed combination and remaining conservative against all admissible alternatives. A tuple can satisfy the former while failing the latter. The disagreement region identifies exactly where this matters for a specified demand inequality, without assuming an actual distribution of demand values.

Resistance nonlinearity and pore pressure can affect a complete stability calculation in ways that are not represented by a local comparison of strength predictions [27]. The discrepancy percentages should consequently not be transferred to factors of safety. A structure samples a spatial stress field; different parts of a potential mechanism may lie on different sides of the crossover. Geometry, drainage and constitutive flow assumptions then influence the response. No finite-element recalculation is performed here. The supported inference is that the material-input choice changes the resistance relation available to such a calculation, not that a particular embankment experiences the same percentage change in stability.

5.3 INTERPRETING THE SCALE OF TABULATED PREDICTION DIFFERENCES

The location of the largest percentage difference need not identify the location of the largest absolute difference. For the TSA comparison, the hybrid input and the stress-rate prediction share the same friction angle and therefore the same transformed slope. Once the stress-rate series becomes the lower mode, their absolute separation remains constant through the upper endpoint. Before the switch, the separation grows because the strain-rate line is steeper than the hybrid. The relative deficit is nevertheless greatest at the switch because the common absolute difference is then divided by a smaller lower-mode resistance than at subsequent coordinates.

For ESA, the selected input follows the strain-rate line and agrees with the lower envelope before the crossover. Above it, the selected line continues with the larger slope while the lower envelope follows the stress-rate prediction. The absolute difference consequently grows with confinement over the remaining domain. This explains why the tabulated upper-endpoint discrepancy is meaningful for that particular comparison. It does not justify comparing the TSA and ESA percentages as if they measured the same material damage or used an interchangeable physical coordinate. Both the reference relation and the coordinate interpretation belong in any tabulated percentage.

Numerical precision should reflect this conditional interpretation. The calculations retain sufficient digits to check the algebra, whereas the main text rounds derived parameters and coordinates for readability. Those extra computational digits do not imply more accurate experimental

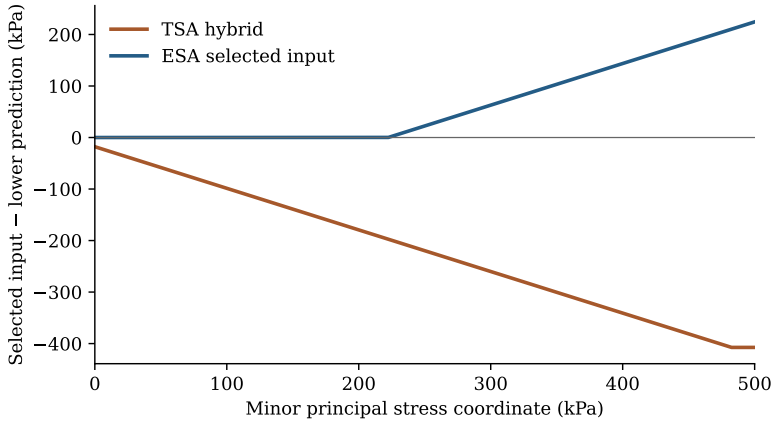


FIGURE 2. SIGNED STRENGTH-SELECTION DIFFERENCES.

measurements. Experimental repeatability must instead be established through independently prepared specimens tested under explicitly matched conditions. Similarly, the exact maximum of a piecewise ratio is a consequence of the admissible lines, not an estimate of an extreme response in an unobserved population. Reporting the domain, active mode and denominator alongside a discrepancy is therefore more informative than giving an isolated percentage or presenting a single value with unjustified physical precision.

The signed differences in Figure 2 separate unnecessary resistance loss from exceedance of the lower loading-mode prediction. Positive values indicate exceedance; negative values indicate a conservative reduction. TSA and ESA retain distinct stress interpretations.

5.4 SINGLE-TUPLE REDUCTION AND ITS COST

For $H = 500$ kPa, the optimal TSA chord is

$$\ell^*_{\mathrm{TSA}}(x) = 153.678570 + 2.661207323x. \tag{19}$$

Its equivalent parameters are $c^* = 40.157915$ kPa and $\phi^* = 34.814867°$. Maximum and mean deficits are 13.963411 and 6.981706 kPa. Unlike componentwise minima, the chord uses both domain endpoints to retain the largest possible mean while remaining below both modes.

The ESA chord is

$$\ell^*_{\mathrm{ESA}}(x) = 499.455353 + 2.241279856x, \tag{20}$$

with $c^* = 138.710204$ kPa and $\phi^* = 31.900398°$. Its sacrifice is

$$g_{\max} = 0.808112265\frac{222.258593(500 - 222.258593)}{500} = 99.770210 \text{ kPa}, \quad \overline{g} = 49.885105 \text{ kPa}. \tag{21}$$

Both chords touch the lower envelope at the endpoints. Endpoint comparisons alone would therefore hide the interior sacrifice. Its size reflects crossover location and slope difference, not an estimated distribution of material error.

The optimisation explains why selecting independent parameter minima need not be efficient even

when conservativeness is the declared objective. Its constraints concern the predicted resistance line, whereas the componentwise rule constrains individual parameters without considering their combined effect over the domain. The endpoint chord satisfies every admissible line inequality while raising the interval-average prediction as far as the admissible affine class permits. Its improved objective value therefore follows from using the complete stress-domain constraint rather than from relaxing conservativeness against the admissible modes.

This result is different from ordinary equivalent-parameter fitting. A least-squares line can cross the target envelope and still provide a small average residual; software documentation explicitly describes equivalent parameters through a stress-range-dependent best fit [17]. The chord is restricted to one side of the lower envelope, and its objective is the average of predicted deviator resistance under uniform confinement weighting. Neither construction is universally preferable. The appropriate choice depends on whether the calculation requires approximation accuracy, a one-sided comparison, compatibility with a constitutive model or another declared purpose. The paper establishes the solution to one such purpose rather than claiming to replace existing fitting practice.

The equivalent cohesion also requires careful interpretation. In ESA, the chord cohesion exceeds the smaller original wet cohesion while its friction angle is lower than that of the corresponding strain-rate series. The resulting prediction still remains below both complete lines. This demonstrates that conservativeness belongs to the relation over the chosen domain, not to a requirement that every equivalent parameter be individually smaller. Parameter dependence therefore remains relevant even in a deterministic reduction. Independent parameter comparisons would miss the compensating effect that the closed-form solution deliberately exploits.

The sacrifice function further identifies where the simplification is least faithful. It vanishes at the endpoints because both endpoint limits are attained by construction, but reaches its maximum at the active-mode intersection. Reporting only endpoint agreement could therefore suggest a closer approximation than exists in the interior. The triangular difference has a direct geometric interpretation, and its mean is half its peak for the two-line case. With more modes the lower envelope can have several active intersections; the same endpoint solution remains valid, but the difference is piecewise linear rather than a single triangle. Its integral must then be calculated using every active segment.

The confinement distribution of the TSA reduction cost is shown in Figure 3. The cost vanishes at the interval endpoints and reaches its maximum at the loading-mode intersection.

The ESA reduction has a broader interior cost distribution (Figure 4). Its area divided by the confinement interval gives the mean resistance sacrifice; this quantity is not mechanical work.

5.5 DOMAIN AND BOUNDED-INPUT SENSITIVITY

Under the illustrative allowance, TSA and ESA crossover coordinates move to 492.8054 and 229.0684 kPa. The smaller TSA deficit in Table 3 is not better material performance: the altered intersection is closer to the upper boundary while the actual predicted resistances are lower.

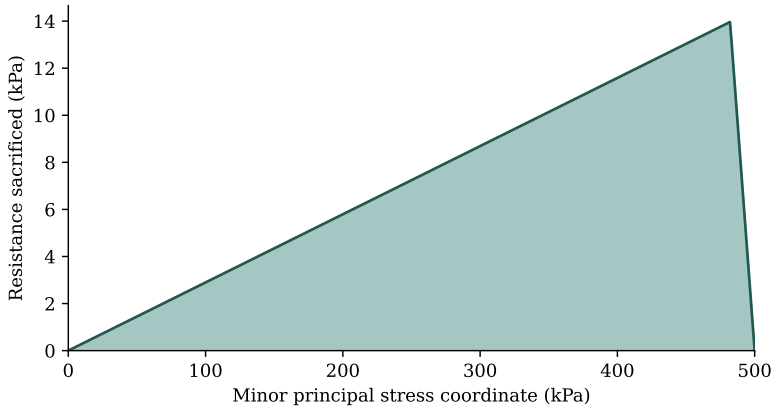


FIGURE 3. TSA RESISTANCE SACRIFICED BY AFFINE REDUCTION.

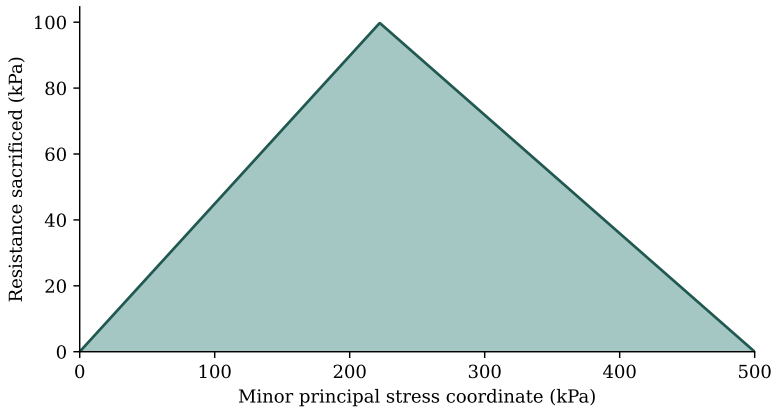


FIGURE 4. ESA RESISTANCE SACRIFICED BY AFFINE REDUCTION.

TABLE 3. DERIVED CONSERVATIVE TUPLES AND PREDICTION DEFICITS FOR $H = 500$ KPA.

Type	Allowance	c^* (kPa)	ϕ^* (°)	$g_{\max}$ (kPa)	$\overline{g}$ (kPa)
TSA	None	40.158	34.815	13.963	6.982
ESA	None	138.710	31.900	99.770	49.885
TSA	5 kPa, 0.5°	35.055	34.426	5.583	2.792
ESA	5 kPa, 0.5°	133.107	31.481	97.730	48.865

Figure 5 varies the ESA domain cap from 100 to 800 kPa and angular allowance from zero to one degree at a fixed 5 kPa cohesion allowance. Caps below the active crossover have zero reduction deficit because one line controls throughout. Including both active modes creates an interior sacrifice. Coordinates beyond the experimental total-confinement range are analytical extrapolation, shown only to expose domain dependence. Mean predicted-resistance deficit of the ESA chord as analytical domain cap and stipulated angular allowance vary.

The sensitivity exercise separates two forms of uncertainty that should not be mixed. Stipulated rectangles allow variation around each mode's tabulated parameters. The dry-state discrepancy instead supplies alternative locations in the publication with different stated values. The former is an analyst-declared allowance; the latter is a feature of the source record. Neither is estimated as a probability distribution. This distinction follows the general need to identify the origin and intended interpretation of an uncertainty statement before propagating it [20, 23].

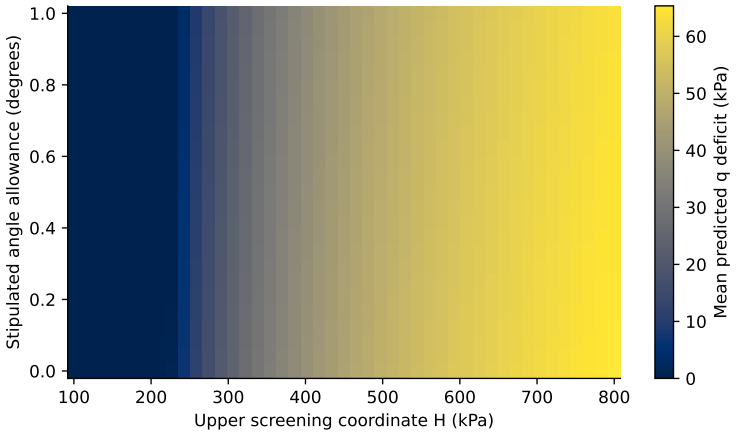


FIGURE 5. MEAN ESA CHORD RESISTANCE DEFICITS ACROSS DOMAIN CAPS AND ALLOWANCES.

A rectangular allowance can be deliberately conservative because it permits within-mode combinations that may not be supported by parameter dependence. Research on joint parameter structures provides reasons to prefer a supported joint set where sufficient observations exist [19]. The rectangle is used here because it is transparent and easy to inspect, not because independence has been demonstrated. Its lower corner is appropriate for the monotonic prediction over nonnegative confinement, but it should not be described as a lower confidence limit. A statistical lower bound would require a sampling model, an estimation procedure and a stated coverage property.

The domain surface also reveals that a reduction cost is not a direct measure of experimental uncertainty. Below a mode crossover, the lower envelope already coincides with one affine prediction and the chord loses nothing. That zero says only that the admissible representation is already linear over the chosen interval. It does not indicate a perfectly measured material or eliminate source inconsistency. Conversely, a larger difference can arise merely because the domain contains substantial portions of two differently sloped lines. The calculated surface is therefore a diagnostic of representation cost conditioned on the input set, not a map of intrinsic soil variability.

The dependence of the equivalent friction angle on interval selection is shown in Figure 6. An interval ending before a mode switch reproduces the controlling line; beyond the switch, the endpoint chord changes continuously with the upper coordinate.

5.6 ALTERNATIVE REPORTING CHANGES RETENTION

The dry TSA alternatives do not affect the wet crossovers or chords. They do change wet/dry retention. For stress-rate control, retention at $x = 0$ is 0.428484 using the summary and 0.372104 using the narrative; at 500 kPa the values are 0.568052 and 0.529150. For strain-rate control, zero-coordinate values are 0.111111 and 0.097561, with upper-endpoint values 0.549362 and 0.513224. These are alternative interpretations of unresolved reporting, not replicate measurements.

ESA stress-rate retention varies from 0.679806 to 0.691168 over the analytical domain, while strain-rate retention varies from 0.448276 to 0.750041. A single percentage reduction in cohesion cannot represent all these predicted resistance ratios. None separates suction changes, fabric

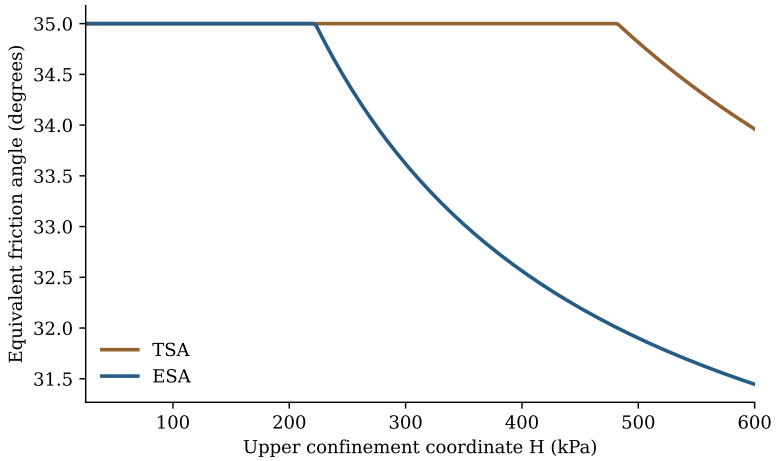


FIGURE 6. FRICTION ANGLE VERSUS CONFINEMENT INTERVAL.

damage and preparation differences causally.

Retention calculations are particularly sensitive to how the reference state is identified. Changing the dry denominator changes the tabulated ratio even when the wet prediction is unchanged. This is why the alternative dry values must be admissible rather than averaged without justification. An average would create another unreported parameter and could conceal the reporting conflict. The separate calculations instead show the practical scale of the ambiguity while leaving its resolution to the original observations or an authoritative correction.

A confinement-dependent retention ratio also differs from a durability index obtained through a specified exposure protocol. Work on cement-treated soils shows that wetting and drying history, additives and binder content influence measured performance [28, 29]. Studies of stabilized expansive subgrades likewise examine both durability and microstructural changes rather than treating an initial strength increment as sufficient evidence [30]. Those findings support caution about interpreting one inundation contrast as a long-term degradation law. They do not establish how the present material would respond to additional cycles, drainage, freeze–thaw action or chemical alteration.

The available record does not identify how much of the wet/dry difference is due to a changed stress state and how much is due to structural alteration. A ratio derived from the fitted lines combines whatever effects are embedded in those lines. Separating mechanisms would require a more controlled design, compatible stress paths and measurements that track the material through exposure. No causal fraction is assigned. This restraint is important because a numerically smaller retention value can be produced by a larger reference strength as well as by a smaller post-exposure strength.

5.7 MEANING OF THE COMBINED ANALYSIS

Selecting the mode with smaller cohesion does not necessarily preserve lower predicted resistance throughout a pressure domain. Componentwise minima can also be more conservative than necessary under a declared mean-resistance objective. The chord theorem provides an alternative

whose interior cost is explicit. Its guarantee concerns a finite model set, not the behaviour of every specimen.

TSA and ESA remain distinct interpretations rather than interchangeable physical corrections. Partially saturated fill can have suction histories not maintained during loading. Preserving that qualification is essential. Likewise, the confinement integral defining the reduction objective is not the strain integral measuring external work. Keeping both levels in the paper does not justify inferring one from the other.

The admissible curve methods would support future joint validation: a conservative peak-strength input could be tested against the recorded resistance through deformation. That analysis requires raw curves with verified measurement conventions. It is not supplied by tabulated cohesion and friction. The tabulated-parameter calculations consequently supply evidence at the model-comparison level while leaving the physical validation of complete stress–strain response unresolved.

The wider ground-improvement literature reinforces the need for this separation of evidence levels. Curing stress can alter the compression behaviour of cement-treated sediment [31]. Initial porosity and water-to-binder relationships have also been used to describe strength, stiffness and durability jointly [32]. These studies indicate that identical binder labels or nominal dosages do not ensure mechanically identical material states. The present calculation therefore preserves mode and state labels instead of pooling their fitted outputs into a single average soil. Additional physical descriptors could refine the admissible set, but cannot be reconstructed from the tabulated parameters alone.

A model of cemented-soil deformation addresses a substantially richer task. Stress-path experiments, stress–dilatancy analysis and constitutive descriptions of cementation examine how resistance evolves with deformation and bond degradation [14–16]. A recent review of biocemented-soil mechanics similarly identifies modelling and scale transfer as important challenges [33]. The chord construction should not be mistaken for such an evolving constitutive law. It supplies a conservative affine peak-resistance relation over a specified coordinate interval; elasticity, flow rule, post-peak response and hydraulic coupling still require separate evidence and modelling decisions.

There is also a difference between a convenient laboratory protocol and a service-relevant validation. New durability procedures explicitly address moisture exposure in combination with cyclic loading [34]. Earlier studies of hydric cycling demonstrate that protocol severity can affect the apparent degradation of stabilized soils [8, 9]. These findings suggest that validation of the present reduction should use a loading and exposure sequence chosen for the intended application, rather than whichever test most readily reproduces a favourable parameter pair. Such validation could establish whether the admissible model alternatives adequately cover an engineering response; it is not supplied by the current parameter comparison.

For decision making, the lower mode envelope is useful because it makes one limited source of ambiguity visible. It can identify a region where a selected input is not conservative relative to another admissible interpretation of the same programme. It cannot absorb every source of geotechnical uncertainty. Spatial variability, construction variability, parameter transformation,

constitutive discrepancy and incomplete environmental histories remain distinct concerns [20, 24]. Assigning a conservative tuple does not remove those concerns or create a quantified reliability level. A defensible design process would preserve them separately and assess how each influences the particular response of interest.

5.8 VERIFICATION AND CALCULATION VERIFICATION

The code reads 14 source-location records, transforms complete tuples, evaluates exact crossover candidates and solves independent endpoint-constrained linear programmes. Both nominal optimisers recover the closed-form chords. One hundred generated affine-line collections also check chord feasibility on a numerical grid. These are mathematical checks, not extra experimental samples; the continuous-domain proof is given in Section 4.

For the admissible integration routine, a declared mathematical function uses nodes $e = (0, 0.01, 0.02, 0.04)$ and ordinates $(0, 120, 150, 90)$ kPa. Its trapezoidal work is 4.35 kJ/m^3. Enumerating every nodal error corner of ± 3 kPa gives $[4.23, 4.47]$ kJ/m^3, agreeing with Eq. (3). It is not an empirical test record or a replacement for unavailable fill measurements.

The accompanying package provides one LaTeX source, compiled PDF, vector and raster figures, transcribed parameter records, exact outputs, source publication, parameter origin information and executable calculations. Main-text Section 3 retains the original methods, and Section 4 integrates the added derivations and proof. No separate appendix is needed.

5.9 A VALIDATION ROUTE CONSISTENT WITH THE AVAILABLE EVIDENCE

A stronger empirical assessment would begin by recovering the original failure observations and matching each observation to its specimen, preparation batch, water state and loading procedure. The fitted tuples could then be reproduced using a documented regression method. Residual analysis would indicate whether a common variance assumption is supportable and whether parameter dependence is represented adequately. Methods designed for shear-parameter estimation and covariance handling would become applicable at that stage [18, 25]. Until then, refitting cannot be replaced by treating the publication's parameter summaries as if they were the original test points.

Verification of effective stress requires its own evidence. Recorded pore pressures, saturation checks and the treatment of suction during shearing should support the coordinate used in the transformed relation. Rate-dependent unsaturated-soil studies show why those measurements cannot be separated casually from the imposed loading sequence [12, 26]. If the coordinate cannot be verified, a sensitivity analysis can still describe consequences of an assumed interpretation, but must retain that conditional status. The numerical precision of an analytically calculated crossover does not improve the physical accuracy of the stress coordinate supplied to it.

Independent validation should then examine a response beyond the observations used to choose or fit the tuples. Suitable responses could include a different controlled confinement path or a

boundary-value experiment whose geometry and loading are known. The aim would be to test whether the reduced input remains adequately conservative for the declared purpose, not simply whether the algebra is reproduced. Because the optimum changes with domain and objective, the validation should document both before evaluation. Additional exposure cycles or another material composition would test transfer, whereas repeated calculations using unchanged tuples would test only numerical consistency.

The distinction between numerical verification and physical validation is central to interpreting the present contribution. The independent linear programme, analytic proof and generated checks show that the reduction problem is solved correctly under its assumptions. They do not show that the assumptions span every relevant state of improved fill. A transparent report should therefore present the result as a conditional tool for input selection, accompanied by the evidence needed to make that condition credible. This is a stronger and more useful claim than either an unsupported declaration of safety or a refusal to calculate anything from incomplete but clearly delimited information.

6. CONCLUSION

Measured wet-state modes change their lower predicted resistance at 482.08 kPa under TSA and 222.26 kPa under the tabulated ESA parameterization. A mode selected by cohesion alone therefore need not remain conservative across the declared confinement interval. The selected TSA hybrid is up to 28.09% below the lower mode prediction, whereas the selected ESA input exceeds its lower mode prediction by 13.85% at 500 kPa. These are parameter-selection effects rather than measured field errors. Separate dry-cohesion reporting alternatives change wet/dry retention and must not be silently reconciled. The endpoint chord is the unique conservative affine prediction maximising interval-average resistance. For 0–500 kPa, equivalent tuples are approximately $(40.158\ \text{kPa}, 34.815^\circ)$ and $(138.710\ \text{kPa}, 31.900^\circ)$, with mean sacrifices of 6.982 and 49.885 kPa. These optima are domain-specific reductions, not new characteristic material strengths. Curve-level work methods remain intact, while parameter-location checking, mode envelopes and conservative reduction add a distinct parameter-level question and calculable results. Applying both layers to verified raw observations and an independent engineering response remains the next empirical requirement.

CONFLICTS OF INTEREST

The authors declare that they have no conflicts of interest related to this research.

DATA AVAILABILITY

The data supporting the findings of this study are available from the corresponding author upon reasonable request.

FUNDING INFORMATION

The authors received no external funding for this research.

REFERENCES

1. Głuchowski, A., Gabryś, K., Soból, E., Šadzevičius, R., and Sas, W. (2020). Geotechnical Properties of Anthropogenic Soils in Road Engineering. *Sustainability*, 12(12), 4843. https://doi.org/10.3390/su12124843.
2. Suescum-Morales, D., Romero-Esquinas, Á., Fernández-Ledesma, E., Fernández, J. M., and Jiménez, J. R. (2019). Feasible use of colliery spoils as subbase layer for low-traffic roads. *Construction and Building Materials*, 229, 116910. https://doi.org/10.1016/j.conbuildmat.2019.116910.
3. Dandin, S., Kulkarni, M., Wagale, M., and Sathe, S. (2022). A review on the geotechnical response of fly ash-colliery spoil blend and stability of coal mine dump. *Cleaner Waste Systems*, 3, 100040. https://doi.org/10.1016/j.clwas.2022.100040.
4. Ohenoja, K., Pesonen, J., Yliniemi, J., and Illikainen, M. (2020). Utilization of Fly Ashes from Fluidized Bed Combustion: A Review. *Sustainability*, 12(7), 2988. https://doi.org/10.3390/su12072988.
5. Barman, D., and Dash, S. K. (2022). Stabilization of expansive soils using chemical additives: A review. *Journal of Rock Mechanics and Geotechnical Engineering*, 14(4), 1319–1342. https://doi.org/10.1016/j.jrmge.2022.02.011.
6. Mugambi, M. L., Toeri, J. R., Kinoti, I. K., Bedada, K. D., and Marangu, J. M. (2023). A Comprehensive Review on Methods, Agents and Durability Factors for Stabilization of Expansive Soils. *Journal of Sustainable Construction Materials and Technologies*, 8(4), 319–343. https://doi.org/10.47481/jscmt.1343552.
7. Krysiak, Ł., Kledyński, Z., and Machowska, A. (2023). Mixtures of colliery spoils and fluidized bed bottom ash: strength and swelling behavior under compressive stress in isolated conditions. *Bulletin of Engineering Geology and the Environment*, 82(5), 164. https://doi.org/10.1007/s10064-023-03200-9.
8. Wassermann, A., Abdallah, A., and Cuisinier, O. (2022). Impact of wetting and drying cycles on the mechanical behaviour of a cement-treated soil. *Transportation Geotechnics*, 36, 100804. https://doi.org/10.1016/j.trgeo.2022.100804.
9. Cuisinier, O., Masrouri, F., and Mehenni, A. (2020). Alteration of the Hydromechanical Performances of a Stabilized Compacted Soil Exposed to Successive Wetting–Drying Cycles. *Journal of Materials in Civil Engineering*, 32(11), 04020349. https://doi.org/10.1061/(asce)mt.1943-5533.0003270.

10. Ding, L. q., Vanapalli, S. K., Zou, W. l., Han, Z., and Wang, X. q. (2021). Freeze-thaw and wetting-drying effects on the hydromechanical behavior of a stabilized expansive soil. *Construction and Building Materials*, 275, 122162. https://doi.org/10.1016/j.conbuildmat.2020.122162.

11. Hu, T., Liu, D., and Chang, J. (2020). Experimental study on strain rate effect of strength characteristics of unsaturated silty clay. *Case Studies in Construction Materials*, 12, e00332. https://doi.org/10.1016/j.cscm.2020.e00332.

12. Wu, S., Zhou, A., Shen, S. L., and Kodikara, J. (2020). Influence of different strain rates on hydro-mechanical behaviour of reconstituted unsaturated soil. *Acta Geotechnica*, 15(12), 3415–3431. https://doi.org/10.1007/s11440-020-01026-3.

13. Zhao, Y., Li, X., and Liu, L. (2025). Measurement of unsaturated soil shear strength through drained-vented triaxial tests. *Journal of Rock Mechanics and Geotechnical Engineering*, 17(9), 5709–5727. https://doi.org/10.1016/j.jrmge.2025.02.026.

14. Landivar Macias, A., and Rotta Loria, A. F. (2023). SANISAND-C*: Simple ANIsotropic constitutive model for SAND with Cementation. *International Journal for Numerical and Analytical Methods in Geomechanics*, 47(15), 2815–2847. https://doi.org/10.1002/nag.3602.

15. Kandasami, R. K., Singh, S., and Murthy, T. G. (2021). Experimental Investigations of the Stress Path Dependence of Weakly Cemented Sand. *Journal of Geotechnical and Geoenvironmental Engineering*, 147(4), 04021007. https://doi.org/10.1061/(asce)gt.1943-5606.0002475.

16. Szypcio, Z., and Dołżyk-Szypcio, K. (2022). The Stress-Dilatancy Behaviour of Artificially Bonded Soils. *Materials*, 15(20), 7068. https://doi.org/10.3390/ma15207068.

17. Rocscience (n.d.). Equivalent Mohr-Coulomb parameters. *RSData Documentation*. https://www.rocscience.com/help/rsdata/documentation/materials/strength-criterion/equivalent-mohr-coulomb-parameters. Accessed 1 November 2026.

18. Brzeziński, K., Józefiak, K., and Zbiciak, A. (2021). On the interpretation of shear parameters uncertainty with a linear regression approach. *Measurement*, 174, 108949. https://doi.org/10.1016/j.measurement.2020.108949.

19. He, R., Wu, C., Xing, X., and Li, J. (2021). Dependence Structures of Soil Parameters in Sandy Clay. *ASCE-ASME Journal of Risk and Uncertainty in Engineering Systems, Part A: Civil Engineering*, 7(3), 05021005. https://doi.org/10.1061/ajrua6.0001158.

20. Phoon, K. K., Cao, Z. J., Ji, J., Leung, Y. F., Najjar, S., Shuku, T., Tang, C., Yin, Z. Y., Ikumasa, Y., and Ching, J. (2022). Geotechnical uncertainty, modeling, and decision making. *Soils and Foundations*, 62(5), 101189. https://doi.org/10.1016/j.sandf.2022.101189.

21. Szczepański, T., Krysiak, Ł., Kiełbasiński, K., and Kaczmarek, Ł. (2025). The impact of water inundation on the geotechnical behavior of artificially made soil from waste materials: contrasting results in total and effective stress analysis. *Mendeley Data*, version 2, accession 8xfppn9j5j. https://doi.org/10.17632/8xfppn9j5j.2. Released 11 October 2025; metadata accessed 1 November 2026; raw files not downloaded.

22. Szczepański, T., Krysiak, Ł., Kiełbasiński, K., and Kaczmarek, Ł. (2025). The impact of water inundation on the geotechnical behaviour of artificial soil made from waste materials: contrasting results in total and effective stress analysis. *Acta Geologica Polonica*, 75(4), e61. https://doi.org/10.24425/agp.2025.157026.

23. Joint Committee for Guides in Metrology (2023). Guide to the expression of uncertainty in measurement—Part 1: Introduction. *JCGM GUM-1:2023*. https://doi.org/10.59161/JCGMGUM-1-2023. Bureau International des Poids et Mesures.

24. Pieczyńska-Kozłowska, J., Bagińska, I., and Kawa, M. (2021). The Identification of the Uncertainty in Soil Strength Parameters Based on CPTu Measurements and Random Fields. *Sensors*, 21(16), 5393. https://doi.org/10.3390/s21165393.

25. Chi, H., Wang, H., Jia, Y., and Zou, D. (2025). A Method for Determining the Soil Shear Strength by Eliminating the Heteroscedasticity and Correlation of the Regression Residual. *Applied Sciences*, 15(18), 10289. https://doi.org/10.3390/app151810289.

26. Wang, H., and Cui, Y. J. (2024). A viscoplastic constitutive model for unsaturated soils based on nonstationary flow surface theory. *International Journal for Numerical and Analytical Methods in Geomechanics*, 48(2), 476–495. https://doi.org/10.1002/nag.3648.

27. Wu, D., Wang, Y., Zhang, F., and Qiu, Y. (2021). Influences of Pore-Water Pressure on Slope Stability considering Strength Nonlinearity. *Advances in Civil Engineering*, 2021(1), 8823899. https://doi.org/10.1155/2021/8823899.

28. Arifin, Y. F., Agustina, E., Andhi, F., and Agus, S. S. (2021). The Role of Additives in Soil-Cement Subjected to Wetting-Drying Cycles. *Infrastructures*, 6(3), 48. https://doi.org/10.3390/infrastructures6030048.

29. Aziz, M., Sheikh, F. N., Qureshi, M. U., Rasool, A. M., and Irfan, M. (2021). Experimental Study on Endurance Performance of Lime and Cement-Treated Cohesive Soil. *KSCE Journal of Civil Engineering*, 25(9), 3306–3318. https://doi.org/10.1007/s12205-021-2154-7.

30. Abbey, S. J., Amakye, S. Y. O., Eyo, E. U., Booth, C. A., and Jeremiah, J. J. (2023). Wet–Dry Cycles and Microstructural Characteristics of Expansive Subgrade Treated with Sustainable Cementitious Waste Materials. *Materials*, 16(8), 3124. https://doi.org/10.3390/ma16083124.

31. He, X., Chen, Y., Wan, Y., Liu, L., and Xue, Q. (2020). Effect of Curing Stress on Compression Behavior of Cement-Treated Dredged Sediment. *International Journal of Geomechanics*, 20(11), 04020204. https://doi.org/10.1061/(asce)gm.1943-5622.0001857.

32. Baldovino, J. A., Nuñez de la Rosa, Y. E., and Palma Calabokis, O. (2023). Analysis of Novel Porosity–Water-to-Binder Index for Prediction of Strength, Stiffness and Durability for Cemented Soils. *Materials*, 16(19), 6354. https://doi.org/10.3390/ma16196354.

33. Harran, R., Terzis, D., and Laloui, L. (2023). Mechanics, Modeling, and Upscaling of Biocemented Soils: A Review of Breakthroughs and Challenges. *International Journal of Geomechanics*, 23(9), 03123004. https://doi.org/10.1061/ijgnai.gmeng-8446.

34. Bazarbekova, A., Kim, Y. R., Little, D. N., and Rushing, J. F. (2025). Novel Test to Assess Moisture-Induced Durability of Stabilized Soils Under Cyclic Loading. *Transportation Research Record: Journal of the Transportation Research Board*, 2679(9), 579–590. https://doi.org/10.1177/03611981251339167.